Title
Water column methanotrophy controlled by a rapid oceanographic switch

Permalink
https://escholarship.org/uc/item/3ng3s41t

Journal
Nature Geoscience, 8(5)

ISSN
1752-0894

Authors
Steinle, Lea
Graves, Carolyn A
Treude, Tina
et al.

Publication Date
2015-05-01

DOI
10.1038/ngeo2420

Peer reviewed

Water column methanotrophy controlled by a rapid oceanographic switch

Lea Steinle[1,2]*, Carolyn A. Graves[3], Tina Treude[2†], Bénédicte Ferré[4], Arne Biastoch[2],
Ingeborg Bussmann[5], Christian Berndt[2], Sebastian Krastel[6], Rachael H. James[3], Erik Behrens[2,7],
Claus W. Böning[2], Jens Greinert[2,4,8†], Célia-Julia Sapart[9,10], Markus Scheinert[2], Stefan Sommer[2],
Moritz F. Lehmann[1] and Helge Niemann[1]*

**Large amounts of the greenhouse gas methane are released
from the seabed to the water column[1], where it may be
consumed by aerobic methanotrophic bacteria[2]. The size and
activity of methanotrophic communities, which determine
the amount of methane consumed in the water column,
are thought to be mainly controlled by nutrient and redox
dynamics[3–7]. Here, we report repeated measurements of
methanotrophic activity and community size at methane
seeps west of Svalbard, and relate them to physical water
mass properties and modelled ocean currents. We show
that cold bottom water, which contained a large number of
aerobic methanotrophs, was displaced by warmer water with a
considerably smaller methanotrophic community within days.
Ocean current simulations using a global ocean/sea-ice model
suggest that this water mass exchange is consistent with
short-term variations in the meandering West Spitsbergen
Current. We conclude that the shift from an offshore to a
nearshore position of the current can rapidly and severely
reduce methanotrophic activity in the water column. Strong
fluctuating currents are common at many methane seep
systems globally, and we suggest that they affect methane
oxidation in the water column at other sites, too.**

Large amounts of methane are stored in the subsurface of
continental margins as solid gas hydrates, gaseous reservoirs or
dissolved in pore water[8]. At cold seeps, various physical, chemical
and geologic processes force subsurface methane to ascend along
pathways of structural weakness to the sea floor, where a portion
of this methane is used by anaerobic and aerobic methanotrophic
microbes[1,9]. On a global scale, about 0.02 Gt yr^{-1} (3–3.5% of the
atmospheric budget[10]) of methane bypasses the benthic filter system
and is liberated to the ocean water column[1], where some of it
is oxidized aerobically (aerobic oxidation of methane—MOx)[2], or
less commonly where the water column is anoxic, anaerobically
(anaerobic oxidation of methane—AOM)[2,11]. MOx is performed
by methanotrophic bacteria (MOB), typically belonging to the
Gamma- (type I) or Alphaproteobacteria (type II)[12,13] according to
the reaction:

$$CH_4 + 2O_2 \rightarrow CO_2 + 2H_2O$$
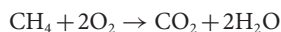
Water column MOx is consequently the final sink for methane
before its release to the atmosphere, where it acts as a potent
greenhouse gas. The water column MOx filter could become more
important in the future because environmental change may induce
bottom water warming, which in turn may accelerate release
of methane from the sea floor[14], in particular along the Arctic
continental margins[15]. Despite the paramount importance of MOx
for mitigating the release of methane to the atmosphere, little
is known about environmental controls on the efficiency of the
water column filter system. Known important factors determining
the structure, activity and size of MOx communities are the
availability of methane[5–7] and oxygen[3], or the abundance of trace
metals (for example, iron and copper)[4,7]. Moreover, evolutionary
adaptations to specific environmental conditions select for certain
types of methanotroph[13]. In addition to environmental selection,
the physical transport of water masses harbouring distinct microbial
communities has been identified as an important factor in shaping
the biogeography of prokaryotic communities[16]. However, the
potential effects of advective processes on the distribution of
methanotrophs and the efficiency of the water column MOx filter
system remain unconstrained[11,17,18].

During two research cruises to the Svalbard continental margin
with R/V *Poseidon* (cruise POS419) and R/V *Maria S. Merian*
(cruise MSM21/4) in August 2011 and 2012, respectively, we
investigated methane dynamics and the activity levels and size
of the water column MOx community in relation to water mass
properties (Fig. 1). The Svalbard margin hosts an extensive,
elongated (~22 km) cold-seep system that is influenced by gas
hydrates (Fig. 1a)[19]. Numerous gas flares emanate from the sea
floor between the 350 and 400 m isobaths[19,20], which corresponds
to the landward termination of the gas hydrate stability zone.
Seep sites have also been mapped on the shelf[19–21], and elevated
methane levels have been observed in several of the fjords in the
Svalbard archipelago[6,22,23].

The hydrodynamics west of Svalbard are governed by the
West Spitsbergen Current (WSC), a 100-km-wide branch of the
Norwegian Atlantic Current, which transports large amounts (up
to 10 Sv) of warm and salty Atlantic Water (AW; >1 °C, >35 psu)
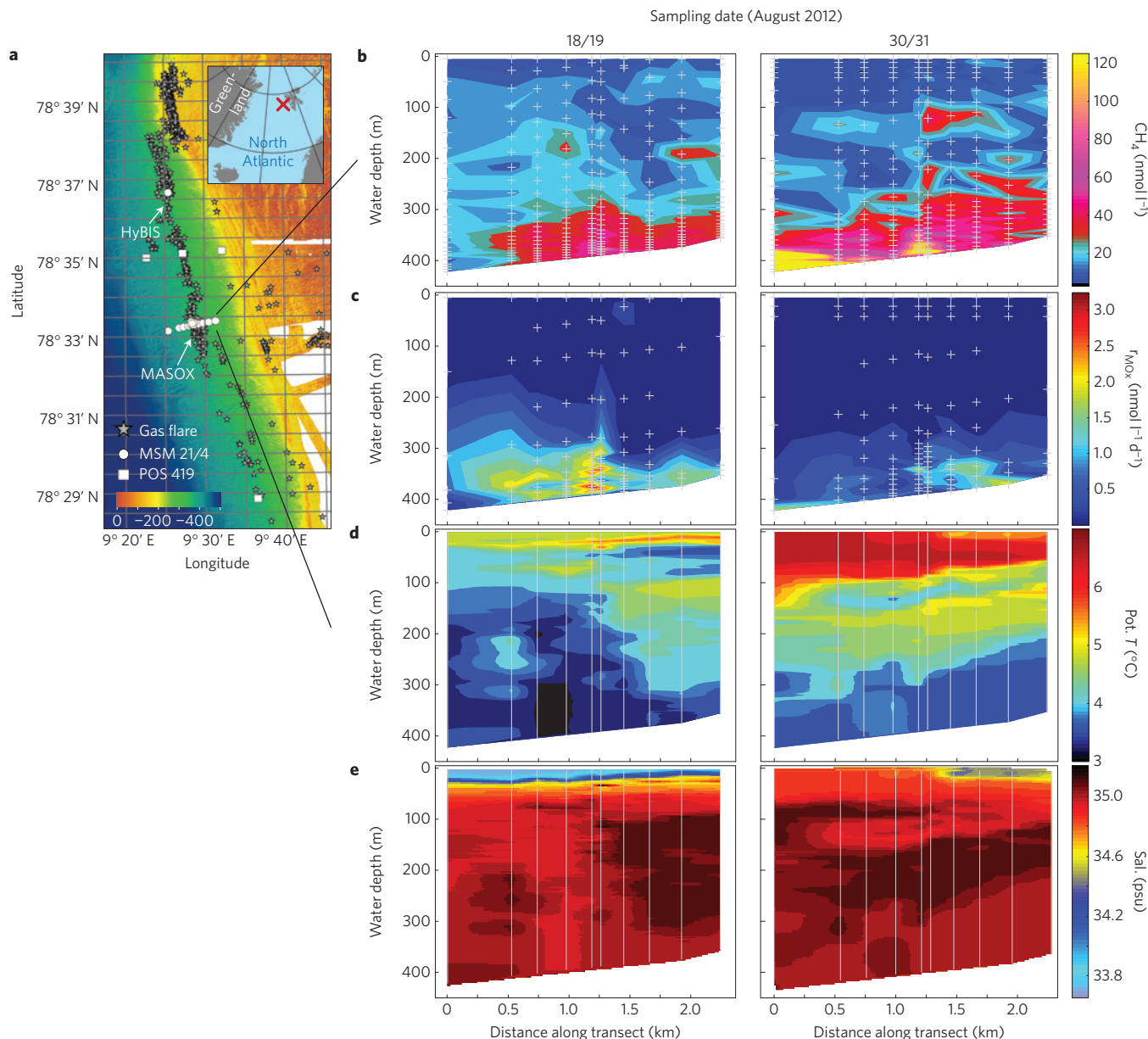northward into the Fram Strait[24]. The WSC flows above cold Arctic

Figure 1 | Study area and distribution of aerobic methanotrophy and physicochemical parameters above methane seeps at the Svalbard continental margin. a, Map of the seep system with numerous methane flares (grey stars) emanating from the sea floor around the depth of the landward termination of the gas hydrate stability zone. Sampling locations are indicated (squares: POS419, 2011; circles: MSM21/4, 2012). **b–e,** Distribution of methane (**b**), aerobic methane oxidation rates (r_{MOx}) (**c**), temperature (**d**) and salinity (**e**) measured during two sampling surveys along the same transect crossing the MASOX site[19]. Positions of discrete samples (crosses) and continuous measurements (lines) are indicated.

Intermediate Water (AIW; <1 °C, ∼34.9 psu; ref. 25). It is steered topographically, and its eastern extension is constrained by the shelf break[26]. East of the WSC on the shelf, the comparably slow East Spitsbergen Current transports cold and relatively fresh Arctic Water (ArW; <3 °C, <34.8 psu) to the north[27].

During two sampling surveys in late August 2012, we measured methane concentrations, MOx activity and MOB abundance, as well as temperature, salinity and oxygen along a transect perpendicular to the line of the methane flares. The two mid-transect stations were at the MASOX site (named after the MASOX Observatory[19]), which is located at 380 m water depth in the centre of the gas flare area both along-slope and down-slope. During both surveys, methane concentrations were highest in bottom waters, frequently exceeding 100 nmol l^{-1} (Fig. 1b). Surface water methane concentrations (9 nmol CH$_4$ l^{-1} on average) were supersaturated by a factor of

∼3 with respect to the local atmospheric equilibrium, indicating methane efflux to the atmosphere from this seep system[19]. Methane dissolved in the water column apparently originates from gas bubbles, which we observed visually during dives with the submersible *Jago*, and which were detected as flares in the middle of the transect with hydroacoustic single-beam systems[19]. Despite the constant supply of methane from the sea floor, we found considerable spatial and temporal variability in MOx activity (Fig. 1c and Supplementary Fig. 1). MOx was highest in bottom waters (>300 m water depth) during the first survey (August 18/19), with methane turnover rates of up to 3.2 nmol l^{-1} d^{-1} (Fig. 1c and Table 1). These rates were similar to maximum rates detected at seeps on the Svalbard shelf[21] and in a nearby fjord[6]. In contrast, overall MOx activity was strongly reduced during the second survey (August 30/31, Fig. 1c and Table 1). Consistent with the
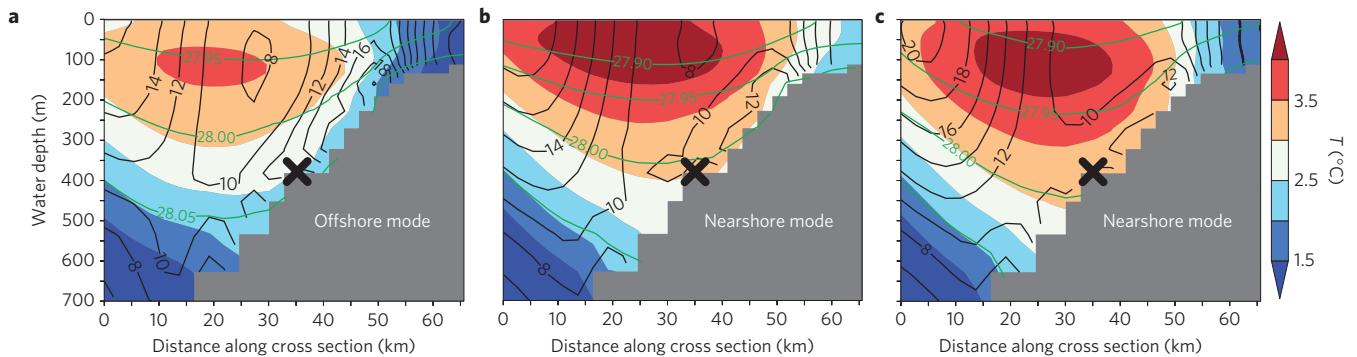
Figure 2 | Modelled cross-slope distribution of water column temperature and current velocity in the West Spitsbergen Current. a–c, Modelled time-averaged water column temperature (°C; colour scale), sigma-t (green contours, kg m^{-3}-1,000) and current velocity (black contours, cm s^{-1}) for cold temperature anomalies (**a**), mean temperature (**b**) and warm temperature anomalies (**c**). Anomalies were defined as one standard deviation below or above the seasonally and interannually varying temperature mean in bottom waters at the MASOX site (cross mark; see Supplementary Fig. 3c). During times of cold temperature anomalies, the WSC is in its offshore mode, with a cold undercurrent along the slope.

MOx activity measurements, cell enumeration conducted in the mid-transect region revealed a maximum in type I MOB cells on August 18/19 (up to 3.0×10^7 cells l^{-1}; Table 1 and Supplementary Fig. 1), but ~75% lower cell numbers during the second survey (up to 7.6×10^6 type I MOB cells l^{-1}). The distributions of MOx activity and MOB cell numbers translate to relatively constant, although low[12,28], cell-specific MOx rates of $1.54–1.66 \times 10^{-2}$ fmol h^{-1} during the two sampling campaigns (Table 1). This constancy suggests that the efficiency of the methanotrophic filter system in the water column was controlled by the size of the MOx community rather than by an environmental stimulus or

suppression mechanism of MOx activity at the organismic level (Supplementary Fig. 2a,b).

Together with the reduction in MOx activity and community size, we observed a strong spatiotemporal change in the distribution of water mass properties. During the August 18/19 survey, bottom waters consisted of cold AW with an admixture of AIW and ArW (Fig. 1d,e), which we subsequently refer to as cold AW (cAW). The cAW has water mass properties (temperature and salinity) akin to those of bottom waters found on the shelf[21]. By August 30/31, the cAW at the bottom was replaced by warmer Atlantic Water (wAW, Fig. 1d,e). As the standing stock of methanotrophs in wAW was much lower than in cAW, rapid water mass exchange constitutes an oceanographic switch, causing a system-wide reduction of the efficiency of water column MOx. This apparent mechanistic link between MOx activity and the presence of either cAW or wAW is reflected in all water column profiles measured in 2012, as well as 2011 (Supplementary Figs 1n and 2c).

We simulated the observed hydrodynamics using the high-resolution (1/20°, ~2.5 km grid space) VIKING20 model, which is nested in the global ocean/sea-ice model ORCA025 and realistically represents ocean circulation variability in the northern North Atlantic[29] (Supplementary Fig. 3). For the WSC, the model yields two modes (offshore and nearshore) with respect to the meandering of the main, warm core of the WSC (Fig. 2 and Supplementary Fig. 3d,e). During the offshore mode, the WSC separates into a warm offshore component and a cold undercurrent, which flows closely along the shelf break. The increase of the undercurrent causes stronger tilts of the isotherms and results in comparably cold bottom water temperatures. As a consequence, bottom waters at the shelf break and on the shelf are of similar density. The ArW on the shelf and fjord waters, both of which are characterized by a high MOx capacity[6,21], can thus be entrained down-slope and contribute to the cAW, a situation that we observed during the August 18/19 survey. As a result, it is plausible that the high standing stock of methanotrophs in cAW partly originates from the shelf. The slow-flowing East Spitsbergen Current and the sheltered fjords lead to comparably long water mass residence times, ensuring continuity of methane supply and supporting MOx community development in the shelf waters. During the nearshore mode, which is representative of the situation that we encountered during the August 30/31 survey, the warm core of the WSC flows closely along the shelf break, replacing the cAW with wAW and separating shelf and deeper AIW. The open-ocean origin of the WSC (ref. 24) makes an exposure to elevated methane concentrations in the history of the wAW unlikely, and could therefore explain the low standing stock of methanotrophs in this water mass.
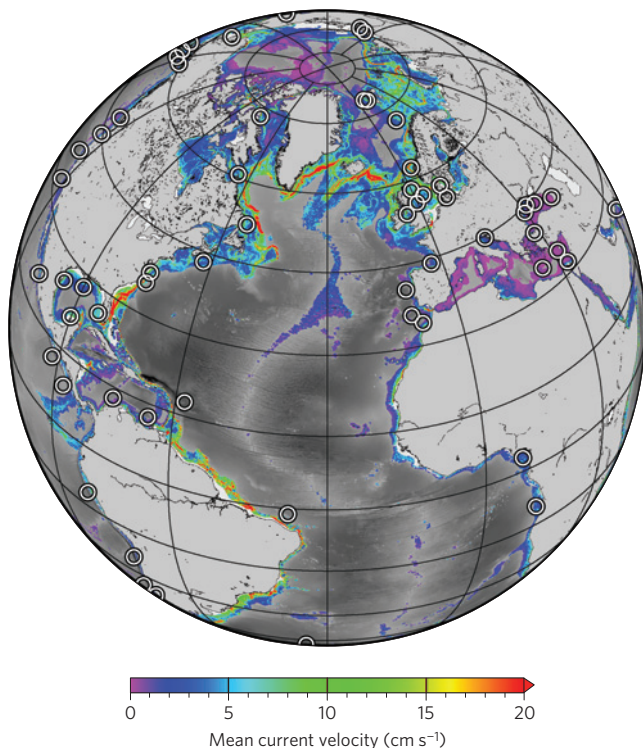

Figure 3 | Modelled bottom water current velocity at methane seeps. Modelled (1/12° resolution) mean annual (year 2000) bottom water current velocities for bottom depths between 100 and 2,500 m. Current velocities at continental margins, where most methane seeps are located, frequently exceed 10 cm s^{-1} and can be highly variable (see Supplementary Fig. 4). White circles indicate locations of selected methane seeps.

Table 1 | Comparison of methane consumption and methanotrophic cell numbers between the two transect sampling campaigns in 2012.

	Sampling date (August 2012)	
	18/19	30/31
Bottom water type	cAW	wAW
WSC mode	Offshore	Nearshore
Max. MOx activity	$3.2\,nmol\,l^{-1}\,d^{-1}$	$2.1\,nmol\,l^{-1}\,d^{-1}$
CH$_4$ oxidized in seep area	$17.82\,kmol\,d^{-1}$ ($0.28\,t\,d^{-1}$)	$5.57\,kmol\,d^{-1}$ ($0.09\,t\,d^{-1}$)
Max. MOB cells	$29.7 \times 10^6\,l^{-1}$	$3.65 \times 10^6\,l^{-1}$
Max. MOB cells (% of tot. cells)	8.3	2.5
Cell-specific MOx activity	$1.54 \pm 0.34 \times 10^{-2}\,fmol\,h^{-1}$ (0.22–$5.74 \times 10^{-2}\,fmol\,h^{-1}$)	$1.66 \pm 0.37 \times 10^{-2}\,fmol\,h^{-1}$ (0.06–$5.66 \times 10^{-2}\,fmol\,h^{-1}$)

Total CH$_4$ oxidized in the seep area was calculated by extrapolation of average MOx rates calculated for each sampling date to the total seep-affected water mass volume (3 km width × 22 km length × 0.388 km average water depth). Highest MOB cell numbers and fraction (in %) of total cell numbers are indicated. Cell-specific MOx rates represent the average of all samples counted on the respective transects (± s.e.m. $n = 12$, August 18/19; $n = 15$, August 30/31).

The dynamics and magnitudes of bottom water temperatures and current velocities simulated by our model correspond well to recorded long-term measurements at the shelf break of the Svalbard margin[19,24]. Modelled and observational data indicate a transition time of 5–10 days between the two described modes. The meandering of the WSC seems to be associated with far-field variations and internal variability of the WSC, but this causality is nonlinear such that the exact timing of the observed switch between the off- and nearshore mode cannot be predicted. Yet, both our model results and measured data from previous work[19,24] indicate that the WSC predominantly flows along the shelf break, whereas the offshore mode, with cAW at the bottom and a high MOx capacity in the water column, occurs only 15% of the time.

At the Svalbard margin, methane flares were observed along a 22-km-long stretch of the upper slope at around 390 m water depth[19,20]. Our model results, together with the measurements of MOx activity and water mass properties, indicate that the entire area is similarly affected by water mass exchange. When spatially extrapolating MOx rate measurements from the transect samplings to the whole seep area (66 km^2), total MOx amounted to 0.28 t CH$_4$ d^{-1} on August 18/19, and was reduced by 66% on August 30/31 (Table 1). Based on the maximum measurements, the capacity of the MOx filter in the studied seep area could well exceed 100 t CH$_4$ yr^{-1}, but this potential remains largely unexploited because the predominant nearshore mode of the WSC reduces MOx capacity to 45 t CH$_4$ yr^{-1}.

Similar to our measurements, varying MOx activities were detected in systems affected by differential circulation patterns and water mass mixing (Black Sea[11]; Santa Monica Basin[18]), and only low water column MOx activities were found at highly active methane seeps influenced by strong bottom currents (Hydrate Ridge[17]; Haakon Mosby Mud Volcano[30]). Currents result in relatively short water mass residence times above methane point sources, so that not enough time and continuity is provided for the development of large methanotrophic communities. Similarly, a well-established MOx community will be swept away from the methane source with the onset of water mass exchange. Dissolved methane, together with the methanotrophic community, will be dispersed leewards, where ongoing MOx activity reduces methane concentrations further[7], most probably at rates controlled by the size of the MOx community. With respect to methane emission to the atmosphere, the impact of currents on water column MOx thus seems strongest in shallow-water cold-seep environments, where the spatiotemporal distance between seafloor methane venting, water column methane consumption and methane evasion to the atmosphere is short. Most methane seeps are located along continental margins, where bottom water currents are commonly strong and fluctuating, as shown by our results from a global, high-resolution circulation model

(ORCA12; Fig. 3 and Supplementary Fig. 4). We thus argue that the variability of physical water mass transport is a globally important control on the distribution and abundance of methanotrophs and, as a consequence, on the efficiency of methane oxidation above point sources.

Methods

Methods and any associated references are available in the online version of the paper.

References

1. Boetius, A. & Wenzhöfer, F. Seafloor oxygen consumption fuelled by methane from cold seeps. *Nature Geosci.* **6,** 725–734 (2013).
2. Reeburgh, W. S. Oceanic methane biogeochemistry. *Chem. Rev.* **107,** 486–513 (2007).
3. Sansone, F. J. & Martens, C. S. Methane oxidation in Cape Lookout Bight, North Carolina. *Limnol. Oceanogr.* **23,** 349–355 (1978).
4. Semrau, J. D., DiSpirito, A. A. & Yoon, S. Methanotrophs and copper. *FEMS Microbiol. Rev.* **34,** 496–531 (2010).
5. Kessler, J. D. *et al.* A persistent oxygen anomaly reveals the fate of spilled methane in the deep Gulf of Mexico. *Science* **331,** 312–315 (2011).
6. Mau, S., Blees, J., Helmke, E., Niemann, H. & Damm, E. Vertical distribution of methane oxidation and methanotrophic response to elevated methane concentrations in stratified waters of the Arctic fjord Storfjorden (Svalbard, Norway). *Biogeosciences* **10,** 6267–6278 (2013).
7. Crespo-Medina, M. *et al.* The rise and fall of methanotrophy following a deepwater oil-well blowout. *Nature Geosci.* **7,** 423–427 (2014).
8. Wallmann, K. *et al.* The global inventory of methane hydrate in marine sediments: A theoretical approach. *Energies* **5,** 2449–2498 (2012).
9. Knittel, K. & Boetius, A. Anaerobic oxidation of methane: Progress with an unknown process. *Annu. Rev. Microbiol.* **63,** 311–334 (2009).
10. Kirschke, S. *et al.* Three decades of global methane sources and sinks. *Nature Geosci.* **6,** 813–823 (2013).
11. Reeburgh, W. S. *et al.* Black-Sea methane geochemistry. *Deep-Sea Res. I* **38,** 1189–1210 (1991).
12. Hanson, R. S. & Hanson, T. E. Methanotrophic bacteria. *Microbiol. Rev.* **60,** 439–471 (1996).
13. Murrell, J. C. in *Handbook of Hydrocarbon and Lipid Microbiology* (ed. Timmis, K. N.) 1953–1966 (Springer, 2010).
14. Ferré, B., Mienert, J. & Feseker, T. Ocean temperature variability for the past 60 years on the Norwegian-Svalbard margin influences gas hydrate stability on human time scales. *J. Geophys. Res.* **117,** C10017 (2012).
15. Biastoch, A. *et al.* Rising Arctic Ocean temperatures cause gas hydrate destabilization and ocean acidification. *Geophys. Res. Lett.* **38,** L08602 (2011).
16. Wilkins, D., van Sebille, E., Rintoul, S. R., Lauro, F. M. & Cavicchioli, R. Advection shapes Southern Ocean microbial assemblages independent of distance and environment effects. *Nature Commun.* **4,** 2457 (2013).
17. Heeschen, K. U. *et al.* Methane sources, distributions, and fluxes from cold vent sites at Hydrate Ridge, Cascadia Margin. *Glob. Biogeochem. Cycles* **19,** GB2016 (2005).

18. Heintz, M. B., Mau, S. & Valentine, D. L. Physical control on methanotrophic potential in waters of the Santa Monica Basin, Southern California. *Limnol. Oceanogr.* **57,** 420–432 (2012).
19. Berndt, C. *et al.* Temporal constraints on hydrate-controlled methane seepage off Svalbard. *Science* **343,** 284–287 (2014).
20. Westbrook, G. K. *et al.* Escape of methane gas from the seabed along the West Spitsbergen continental margin. *Geophys. Res. Lett.* **36,** L15608 (2009).
21. Gentz, T. *et al.* A water column study of methane around gas flares located at the West Spitsbergen continental margin. *Cont. Shelf Res.* **72,** 107–118 (2014).
22. Damm, E., Mackensen, A., Budéus, G., Faber, E. & Hanfland, C. Pathways of methane in seawater: Plume spreading in an Arctic shelf environment (SW-Spitsbergen). *Cont. Shelf Res.* **25,** 1453–1472 (2005).
23. Damm, E., Kiene, R. P., Schwarz, J., Falck, E. & Dieckmann, G. Methane cycling in Arctic shelf water and its relationship with phytoplankton biomass and DMSP. *Mar. Chem.* **109,** 45–59 (2008).
24. Schauer, U., Fahrbach, E., Osterhus, S. & Rohardt, G. Arctic warming through the Fram Strait: Oceanic heat transport from 3 years of measurements. *J. Geophys. Res.* **109,** C06026 (2004).
25. Blindheim, J. Arctic intermediate water in the Norwegian sea. *Deep-Sea Res. I* **37,** 1475–1489 (1990).
26. Bourke, R. H., Weigel, A. M. & Paquette, R. G. The westward turning branch of the West Spitsbergen Current. *J. Geophys. Res.* **93,** 14065–14077 (1988).
27. Loeng, H. Features of the physical oceanographic conditions of the Barents Sea. *Polar Res.* **10,** 5–18 (1991).
28. Carini, S., Bano, N., LeCleir, G. & Joye, S. B. Aerobic methane oxidation and methanotroph community composition during seasonal stratification in Mono Lake, California (USA). *Environ. Microbiol.* **7,** 1127–1138 (2005).
29. Fischer, J. *et al.* Intra-seasonal variability of the DWBC in the western subpolar North Atlantic. *Prog. Oceanogr.* **132,** 233–249 (2015).
30. Sauter, E. J. *et al.* Methane discharge from a deep-sea submarine mud volcano into the upper water column by gas hydrate-coated methane bubbles. *Earth Planet. Sci. Lett.* **243,** 354–365 (2006).

Author contributions

L.S., C.A.G., T.T., I.B., J.G., C-J.S., S.S. and H.N. collected the samples and performed measurements of biogeochemical rates and/or physicochemical parameters. L.S. carried out enumeration of microbial cells. A.B., B.F., J.G., E.B., C.W.B. and M.S. conducted oceanographic modelling, interpretation and/or graphical representation. C.B. and S.K. were responsible for acoustic measurements. T.T., R.H.J., M.F.L. and H.N. supervised research. L.S. and H.N. led the development of the manuscript and all co-authors contributed to data interpretation and writing of the manuscript.

Additional information

Supplementary information is available in the online version of the paper. Reprints and permissions information is available online at www.nature.com/reprints. Correspondence and requests for materials should be addressed to L.S. or H.N.

Competing financial interests

The authors declare no competing financial interests.

Methods

Sampling. To assess the spatiotemporal variability of physical water mass properties, methane concentrations, MOx rates and abundance of methanotrophs, we repeatedly sampled the water column at several stations, most importantly at the MASOX site and/or along a transect crossing this site (Fig. 1a). Discrete values were interpolated linearly for spatial representation of physicochemical and biogeochemical water column parameters.

Physical water mass properties. Temperature and salinity were measured with a Seabird SBE911 CTD (CTD: conductivity/temperature/depth probe; Seabird-Electronics, USA) equipped with dual temperature and conductivity sensors.

Methane concentration, oxidation rates and abundance of methanotrophs. Methane concentrations, MOx rates and community size were determined from aliquots of seawater samples recovered with a CTD/Rosette sampler equipped with 24×10 L PTFE-lined Niskin bottles. Methane was analysed with a headspace technique and gas chromatography with flame ionization detection. MOx rates

were determined at sea from *ex situ* incubations with trace amounts of tritium-labelled methane (^{3}H–CH$_4$). MOB cell numbers were enumerated by using catalysed reporter deposition fluorescence *in situ* hybridization (CARD-FISH) and epifluorescence microscopy.

Oceanographic modelling. To model the hydrodynamics at the continental shelf break offshore Svalbard, we used 5-daily output from the VIKING20 model, a high-resolution ocean/sea-ice model, which is forced by atmospheric data covering synoptic (6-hourly to daily), seasonal, interannual to decadal timescales of the years 1948–2007. Global bottom water velocities at continental margins were analysed using a global variant of the ocean/sea-ice model (ORCA12).

Data availability. All data presented in this paper are available in the PANGAEA data library (http://doi.pangaea.de/10.1594/PANGAEA.844013).

Code availability. The code used for the ORCA12 and VIKING20 models is available on request.